J Appl Math Comput (2011) 36: 401–416
DOI 10.1007/s12190-010-0410-y

JAMC

Combined diffraction and radiation of ocean waves around an OWC device

Song-Ping Zhu · Lewis Mitchell

Received: 19 February 2010 / Published online: 9 June 2010

Abstract In a previous paper we provided an analytical solution for the problem of diffraction of plane surface waves by a suspended hollow cylindrical shell structure. Following on from that work, in this paper we formulate and solve the related problem of radiation of ocean waves by an oscillating surface pressure within the cylinder. We find that the same technique of reducing the problem to an infinite system of linear simultaneous equations can still be employed, and use this technique to find a rapidly converging solution. We present an analysis of convergence and accuracy for the radiation problem, as well as results for the combined diffraction-radiation problem, which we obtain by a linear superposition of the two wave fields.

Keywords Oscillating water column · Wave diffraction and radiation · Renewable wave energy

Mathematics Subject Classification (2000) 76B15

1 Introduction

The study of diffraction and radiation of surface waves around structures has been the subject of renewed interest in recent years due to an increase in study of renewable energy. Oscillating Water Column (OWC) devices present an approach to energy generation that does not produce CO_2 emissions, and is therefore an attractive solution to the problem of "green" electricity generation. In such devices power is generated by incoming plane surface waves which create an oscillating pressure within the cylinder. The wave-induced pressure then forces the oscillatory motion of the air inside of

S.-P. Zhu (✉) · L. Mitchell
School of Mathematics and Applied Statistics, University of Wollongong, Northfield Avenue, Wollongong NSW 2522, Australia
e-mail: spz@uow.edu.au

Fig. 1 An OWC prototype located at Port Kembla, NSW, Australia

a sealed chamber, which drives a specially designed turbine with its blades controlled by a computer and a set of servo motors so that a one directional rotation can be maintained while the air flow is alternating in directions as water surface moves up and down. For example, Oceanlinx Limited Australia has already developed a prototype based on the concept of OWC. Figure 1 displays this prototype, which is currently installed at Port Kembla, NSW, Australia and has successfully converted ocean wave energy into electricity in a number of test runs.

Two of the problems related to optimally designing an OWC plant so that the maximum energy can be efficiently extracted from an incoming wave field are:

1. how to design the shape of the OWC chamber to extract the largest possible oscillating pressure inside the device, and
2. where to position the device in the ocean to capture waves as large as possible, while minimizing the oscillation of the structure itself.

The first point relates to diffraction of incoming plane waves, which has been studied in Zhu and Mitchell [15]. The second relates to the combined wave diffraction and radiation by an oscillating surface pressure inside the cylinder, which is the subject of the current paper.

One should realize that to better understand this system, studying the diffraction of waves by the OWC chamber is not enough, because the turbine's reactional force on the air has created an oscillating surface pressure inside the cylinder. This pressure will then produce waves which radiate outwards from the cylinder. Therefore, not only do we need to study the diffraction problem as we did in Zhu and Mitchell [15], we need to study a radiation problem, which is the subject of this paper.

In Zhu and Mitchell [15] we solved the problem of diffraction of surface waves around a suspended cylindrical shell. Using the same approach in this paper, we present a first-order analytical solution for the problem of surface wave radiation around a hollow suspended cylinder in an ocean of finite depth. By the linearity of the problem, the solution to the combined diffraction-radiation problem is the linear superposition of the diffracted and radiated wave fields.

There have been some published papers on OWC devices since the first studies from the 1970s. Lighthill's early two-dimensional analysis of wave-energy extraction

by a submerged duct [7] was extended by three-dimensional analyses of diffraction around a duct structure in an ocean of infinite depth, courtesy of Simon [12] and Miles [10] in the early 1980s. Later works by Evans [2] and Sarmento and de O. Falcao [11] laid further groundwork for the theory of diffraction and radiation of ocean waves by OWC-like structures in both the linear and non-linear regimes. However, both works were limited to two-dimensional analyses only. In 2004, Hong et al. [6] presented a 3-D numerical model based on solving an integral equation to study the motion and drift forces of a floating OWC device. More recently, Martins-Rivas and Mei [8] studied wave diffraction problem of an OWC installed at the tip of a long and thin breakwater.

Analytical solutions to the combined diffraction-radiation problem have not been found in the literature, except for a brief treatment by Falnes [4], which places more emphasis on the forces on the cylinder rather than on the wave fields themselves, as we shall do here. Although the radiation problem with a hollow cylinder has not previously been studied in detail, the solution to the equivalent problem without a cylinder is well known and is described in Stoker [13] and Wehausen and Laitone [14]. Also, Evans and Porter [3] used a numerical method to calculate the hydrodynamic properties of an OWC device similar to the one we will study, however this method has the disadvantage of being only approximate whereas our solution is analytic and therefore exact. Our approach will follow that used by Garrett [5] for the related diffraction problem.

In Sect. 2 we formulate the problem in terms of an infinite set of linear equations, which is solved by means of the matrix method presented in Sect. 3. In Sect. 4 we present our results and analysis, focussing on the convergence of the solution and how well the boundary conditions are satisfied. We also present results for the combined diffraction-radiation problem. Finally, in Sect. 5 we present our conclusions.

2 Formulation

Obtaining a full analytical solution for the complex geometry of an actual OWC device is a task beyond the scope of this work. For that reason, we make the simplifying assumption that the OWC can be approximated by the geometry of a hollow upright cylinder suspended in an ocean of finite depth. It is also assumed that the suspended hollow cylinder is fixed somewhat by a mooring system and thus it has zero velocity with respect to the ocean floor. All these assumptions of course have made the modeled situation a bit away from the engineering reality. However, they will allow us to obtain an exact solution, which nonetheless has the practical application of giving physical insight into the problem as well as a test case by which to benchmark numerical approaches.

We formulate the problem as follows: consider a time-dependent surface pressure P_0 oscillating with frequency ω applied on the surface inside a hollow cylinder of radius a and zero thickness. The cylinder is suspended at height h above the floor of an ocean of depth d. We fix a coordinate system with the origin coincident with the center of the cylinder on the ocean floor, the z-direction pointing vertically upwards

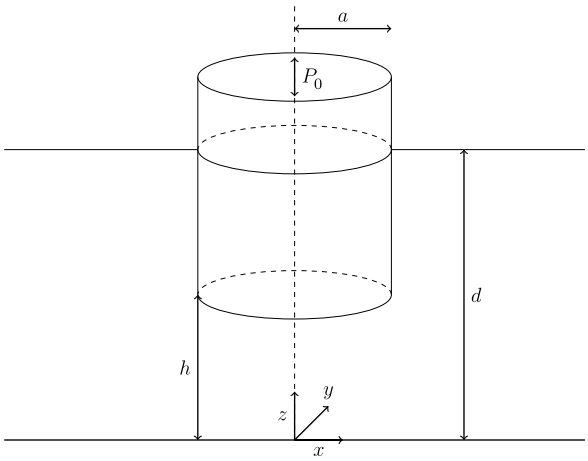

Fig. 2 Schematic diagram

as shown in a schematic diagram of Fig. 2. For the radiation problem under consideration, the direction of the x coordinate is not very crucial. However, for the convenience of later imposition of the solution of diffracted wave field, the x-direction is set along the same direction of the propagation of the incoming waves in the diffraction problem as shown in Fig. 2.

Within the linear theory, we only need to consider the induced wave field by one mode the inner surface pressure oscillation; Fourier decomposition can be easily adopted to analyze the oscillating pressure with multi-frequencies. Under the conventional water wave theory (cf. [9]), the radiated wave potential ϕ satisfies the following differential system with

$$\nabla^2\phi = 0, \tag{1}$$

subject to

$$\frac{\partial\phi}{\partial z} = 0 \quad \text{on } z = 0, \tag{2}$$

$$\frac{\partial\phi}{\partial z} - \frac{\omega^2}{g}\phi = \begin{cases} \frac{i\omega P_0}{\rho g} & \text{if } r \le a \\ 0 & \text{if } r \ge a \end{cases} \quad \text{on } z = d, \tag{3}$$

$$\frac{\partial\phi}{\partial r} = 0 \quad \text{on } r = a, \text{ for } h \le z \le d, \tag{4}$$

$$\sqrt{r}\left(\frac{\partial\phi}{\partial r} - ik\phi\right) \to 0 \quad \text{as } r \to \infty, \tag{5}$$

where ρ is the density of the fluid and g is the acceleration due to gravity. Equations (2) and (4) are zero displacement boundary conditions for the solid ocean floor and cylinder surface respectively, while (3) is the combined kinematic and dynamic free surface condition at the ocean surface. Equation (5) is the Sommerfeld radiation condition, which ensures that the radiated wave is outgoing far away from the cylinder. The calculated wave potential, of course, needs to be multiplied by the time factor

$e^{-i\omega t}$, where t stands for time, in order to obtain the total wave potential $\Phi = \phi e^{-i\omega t}$ and then the velocity, $\overrightarrow{u} = \nabla\phi$, of the entire flow field. Interested readers are referred to [9] for the details of those standard definitions.

We decompose ϕ into two functions defined on $r \le a$ and $r \ge a$, respectively:

$$\phi = \begin{cases} \phi_{\text{int}}, & r \le a, \\ \phi_{\text{ext}}, & r \ge a, \end{cases} \tag{6}$$

and so introduce the continuity conditions

$$\phi_{\text{int}} = \phi_{\text{ext}}, \quad \text{at } r = a \text{ for } 0 \le z \le h, \quad \text{and} \tag{7}$$

$$\frac{\partial \phi_{\text{int}}}{\partial r} = \frac{\partial \phi_{\text{ext}}}{\partial r} \quad \text{at } r = a \text{ for } 0 \le z \le h, \tag{8}$$

which are necessary to close the system.

We write ϕ as

$$\phi(r, z, \theta) = \sum_{m=0}^{\infty} \psi_{m,1}(r, z) \cos m\theta + \psi_{m,2}(r, z) \sin m\theta, \tag{9}$$

and define the surface disturbance

$$\zeta_{\text{int}}(r, \theta) = \sum_{m=0}^{\infty} \chi_{m,\text{int},1}(r) \cos m\theta + \chi_{m,\text{int},2}(r) \sin m\theta, \tag{10}$$

with χ_m and ψ_m related by the kinematic surface condition

$$-i\omega\chi_m(r) = \left.\frac{\partial \psi_m}{\partial z}\right|_{z=d}. \tag{11}$$

Now by separating variables we expand $\psi_{m,\text{int}}$ as

$$\begin{aligned} \psi_{m,\text{int}}(r, z) = {} & [C_1 J_m(kr) + C_2 Y_m(kr)]\, Z_k(z) \\ & + \sum_{\alpha} [C_{1\alpha} I_m(\alpha r) + C_{2\alpha} K_m(\alpha r)]\, Z_\alpha(z), \end{aligned} \tag{12}$$

where C_1, C_2, $C_{1\alpha}$ and $C_{2\alpha}$ are arbitrary constants. A similar expression holds for the function in the exterior region, $\psi_{m,\text{ext}}$, except with different coefficients, so we omit it here. The wavenumbers k and α are determined from the dispersion relations

$$\omega^2 - gk \tanh kd = 0, \tag{13}$$

and

$$\omega^2 + \alpha g \tan \alpha d = 0 \tag{14}$$

respectively. Note that the derivation of the above expression is the same for $\psi_{m,1}$ and $\psi_{m,2}$.

As for the diffraction problem [15], we introduce the eigenfunctions

$$Z_k(z) = N_k^{-\frac{1}{2}} \cosh kz, \tag{15}$$

$$Z_\alpha(z) = N_\alpha^{-\frac{1}{2}} \cos \alpha z, \tag{16}$$

where

$$N_k = \frac{1}{2}\left(1 + \frac{\sinh 2kd}{2kd}\right),$$

$$N_\alpha = \frac{1}{2}\left(1 + \frac{\sin 2\alpha d}{2\alpha d}\right),$$

and expand $\frac{\partial \psi_m}{\partial r}$ over $[0, d]$ as

$$\left.\frac{\partial \psi_m}{\partial r}\right|_{r=a} = \sum_\alpha \mathcal{F}_{m\alpha} Z_\alpha(z), \tag{17}$$

$$\text{where } \mathcal{F}_{m\alpha} = \frac{1}{d}\int_0^h f_m(z) Z_\alpha(z) dz, \tag{18}$$

$$f_m(z) = \frac{\partial \psi_m}{\partial r}, \quad \text{at } r = a, \text{ for } 0 \le z < h. \tag{19}$$

It should be noted that the summation over α in (17) is over all the real as well as the imaginary roots of the dispersion relation, which yields (13) and (14), respectively. Equation (13) corresponds to the propagating mode whereas as all the other roots of (14) give the evanescent modes (cf. [9]).

In the case where P_0 is constant, we make the linear transformation

$$\phi_{\text{int}} = \phi^*_{\text{int}} + \frac{i P_0}{\rho\omega}, \tag{20}$$

so that ϕ^* satisfies the original system (1)–(4), but with the inhomogeneous free surface condition (3) changed to the homogeneous one

$$\frac{\partial \phi^*_{\text{int}}}{\partial z} - \frac{\omega^2}{g}\phi^*_{\text{int}} = 0 \quad \text{on } z = d. \tag{21}$$

In this case the solution proceeds as for the diffraction problem, and so we obtain the expansion for the interior wave field as

$$\phi_{\text{int}}(r, z, \theta) = \sum_{m=0}^{\infty}\sum_\alpha \left[\mathcal{F}_{1m\alpha}\frac{I_m(\alpha r)}{\alpha I'_m(\alpha a)} Z_\alpha(z)\cos m\theta + \mathcal{F}_{2m\alpha}\frac{I_m(\alpha r)}{\alpha I'_m(\alpha a)} Z_\alpha(z)\sin m\theta\right] + \frac{i P_0}{\rho\omega}. \tag{22}$$

For the radially dependent surface pressure case we define the Hankel transform of $P(r)$

$$\mathbf{P}(\kappa) = \int_0^\infty r P(r) J_0(\kappa r) dr,$$

and noting that $P(r)$ is only non-zero on $r \in [0, a]$, obtain an expansion for the interior potential

$$\phi_{\text{int}}(r, z, \theta) = \frac{i\omega}{\rho} PV \int_0^\infty \frac{\kappa \mathbf{P}(\kappa) \cosh \kappa z J_0(\kappa r)}{\kappa g \sinh \kappa d - \omega^2 \cosh \kappa d} d\kappa + \frac{k\mathbf{P}(k) \cosh kz J_0(kr)}{g \sinh kd + kdg \cosh kd - \omega^2 d \sinh kd}, \tag{23}$$

where PV indicates the Cauchy principal value of the integral. In both cases the exterior expansion for the radiation problem is given by

$$\phi_{\text{ext}}(r, z, \theta) = \sum_{m=0}^{\infty} \sum_{\alpha} \left[\mathcal{F}_{1m\alpha} \frac{K_m(\alpha r)}{\alpha K_m'(\alpha a)} Z_\alpha(z) \cos m\theta + \mathcal{F}_{2m\alpha} \frac{K_m(\alpha r)}{\alpha K_m'(\alpha a)} Z_\alpha(z) \sin m\theta \right]. \tag{24}$$

We now have complete expansions for the radiated potential in entire domain, for an arbitrary inner surface pressure distribution. This is significant as it gives us equations for the radiated wave field for either a uniform or non-uniform pressure which could be produced by a rotating turbine. It remains to determine the constants $\mathcal{F}_{1m\alpha}$ and $\mathcal{F}_{2m\alpha}$, which is the subject of the next section.

3 Solution

Having formulated the problem in terms of eigenfunction expansions in the same way as we did for the diffraction problem, we may use the same techniques to obtain the solution as we presented in Zhu and Mitchell [15]. Using the continuity condition (7) as well as the orthogonality of the eigenfunctions Z_α and Z_β we obtain the full solution for the constants $\mathcal{F}_{m\alpha}$ as an infinite system of independent linear equations.

3.1 $P_0 = \text{constant}$

For this case we must perform an eigenfunction expansion of the constant surface pressure inside the cylinder. Using the eigenfunctions Z_α as well as Bessel functions present inside the cylinder we let

$$\frac{iP_0}{\rho\omega} = \sum_{m=0}^{\infty} \sum_{\alpha} \left[P_{m\alpha} I_m(\alpha r) Z_\alpha(z) \cos m\theta + Q_{m\alpha} I_m(\alpha r) Z_\alpha(z) \sin m\theta \right], \tag{25}$$

where

$$P_{m\alpha} = N_P \int_0^d \int_0^a \int_0^{2\pi} \frac{i P_0}{\rho\omega} I_m(\alpha r) Z_\alpha(z) \cos m\theta d\theta dr dz,$$

$$Q_{m\alpha} = N_Q \int_0^d \int_0^a \int_0^{2\pi} \frac{i P_0}{\rho\omega} I_m(\alpha r) Z_\alpha(z) \sin m\theta d\theta dr dz,$$

with

$$N_P = \left[\int_0^d \int_0^a \int_0^{2\pi} I_m^2(\alpha r) Z_\alpha^2(z) \cos^2 m\theta d\theta dr dz \right]^{-1},$$

$$N_Q = \left[\int_0^d \int_0^a \int_0^{2\pi} I_m^2(\alpha r) Z_\alpha^2(z) \sin^2 m\theta d\theta dr dz \right]^{-1}.$$

Substituting (22) and (25) into (7), using the orthogonality of the Z_α's and integrating over the region of validity we obtain

$$\sum_\alpha P_{m\alpha} D_{\beta\alpha} = \sum_\alpha E_{\beta\alpha} \mathcal{F}_{1m\alpha}, \tag{26}$$

where

$$D_{\beta\alpha} = \frac{1}{d} \int_0^h Z_\alpha(z) Z_\beta(z) dz, \tag{27}$$

$$E_{\beta\alpha} = (R_\alpha - 1) D_{\beta\alpha} + \delta_{\beta\alpha}, \tag{28}$$

$$R_\alpha = \left[\alpha^2 a^2 I_m'(\alpha a) K_m'(\alpha a) \right]^{-1}. \tag{29}$$

If we write (26) in a matrix form, we have

$$\mathbf{E} \mathcal{F}_{1m} = \bar{\mathbf{d}}_1, \tag{30}$$

where $\mathbf{E}$ is an $N \times N$ coefficient matrix with entries $\mathbf{E}_{\beta\alpha}$, $\mathcal{F}_{1m}$ is an $N \times 1$ column vector that contains the unknown coefficients for the *mth* mode of the first eigenfunction in (24) and $\bar{\mathbf{d}}_1$ is an $N \times 1$ column vector containing the product values of $\sum_\alpha P_{m\alpha} D_{\beta\alpha}$ for each mode m. This matrix equation resembles very much the final matrix equation we found for the diffraction problem (cf. [15]), and we shall solve it in a similar fashion.

The solution for all the unknown coefficients contained in $\mathcal{F}_{2m}$ is solved similarly too.

3.2 $P_0 = P_0(r)$

Following a similar procedure for the spatially non-uniform surface pressure case, we have

$$F_\beta = \sum_\alpha E_{\beta\alpha} \mathcal{F}_{1m\alpha}, \tag{31}$$

where

$$F_\beta = \frac{i\omega}{\rho d} PV \int_0^\infty \frac{\kappa \mathbf{P}(\kappa) J_0(\kappa a)}{\kappa g \sinh \kappa d - \omega^2 \cosh \kappa d} \int_0^h \cosh \kappa z Z_\beta(z) dz d\kappa + \frac{k \mathbf{P}(k) J_0(ka) N_k^{1/2}}{g \sinh kd + kdg \cosh kd - \omega^2 d \sinh kd} C_\beta, \tag{32}$$

$$C_\beta = \frac{1}{d} \int_0^h Z_k(z) Z_\beta(z) dz, \tag{33}$$

$$D_{\beta\alpha} = \frac{1}{d} \int_0^h Z_\alpha(z) Z_\beta(z) dz, \tag{34}$$

$$E_{\beta\alpha} = (R_\alpha - 1) D_{\beta\alpha} + \delta_{\beta\alpha}, \tag{35}$$

$$R_\alpha = \frac{K_m(\alpha a)}{\alpha K_m'(\alpha a)}, \tag{36}$$

and again the solution for $\mathcal{F}_{2m\alpha}$ follows similarly.

We can formulate (31) as a matrix equation:

$$\mathbf{E}_{\beta\alpha} \mathcal{F}_{1m\alpha} = \mathbf{F}_\beta, \tag{37}$$

which we solve as previously for the desired number of coefficients $\mathcal{F}_{1m\alpha}$ and $\mathcal{F}_{2m\alpha}$.

With this set of coefficients we now have a complete solution for the velocity potential on the entire domain. This means that for any given geometry and inner surface pressure distribution P_0 we may obtain the wave field produced. In a practical application this can give valuable insight into how the device interacts with its surroundings and changes the nearby wave field, which can have obvious engineering applications in assisting design and operation of OWCs. We provide a number of numerical examples for different geometries in the next section.

4 Results

The matrix system presented in the previous section can be numerically solved once the dimension of the system is reduced to a finite number N. In this section, we analyze the rate of convergence and accuracy of the series solution for the radiation problem, focussing on how well the solution matches the boundary conditions, as a sufficient N is taken. In all the results presented in this section, unless otherwise stated, we have used the parameter values $N = 40$, $a = 10$ m, $d/a = 0.6$, $h/a = 0.4$, $P_0 = 100$ Pa, $\omega = 1\ \mathrm{s}^{-1}$ and $\rho = 1\ \mathrm{kg\,m}^{-3}$. SI units are used on the axes of all figures. Note that for the spatially uniform case and for the non-uniform example we will choose, only the first ($m = 0$) mode needs to be calculated. There is however still a summation over the α values to be performed.

It should be noted that through our eigenfunction expansion, all boundary conditions, except for the zero flux boundary condition at $r = a$ (i.e., (4)), are exactly

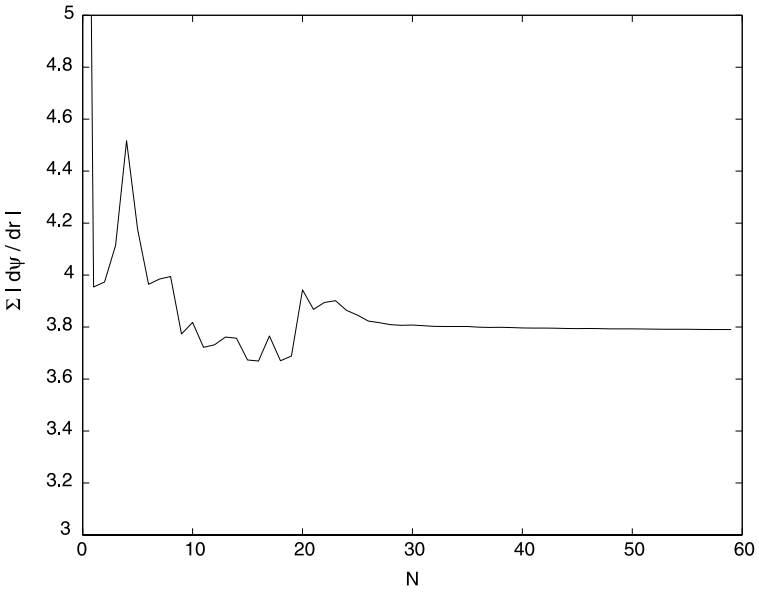

Fig. 3 Error in $\frac{\partial \phi}{\partial r} = 0$ boundary condition matching for $h \leq z \leq d$, $r = a$ as a function of N

satisfied. Therefore, we only need to examine the satisfaction of (4), in order to examine the degree of the accuracy of our solution. This is achieved by examining an error measure designed to measure the collective difference of how much $\frac{\partial \psi}{\partial r}$ deviates from zero on the surface of the cylinder $h \leq z \leq d$.

Figure 3 shows the variation of such a measure, $\| \frac{\partial \psi}{\partial r} \|$, defined by

$$\left\| \frac{\partial \psi}{\partial r} \right\| = \sum_{m=0}^{N} \int_h^d \left| \frac{\partial \psi_m}{\partial r} \right|_{r=a} dz, \tag{38}$$

as a function of the maximum number of modes summed upto N. Clearly, this measure represents the total absolute area underneath the curve $\frac{\partial \psi}{\partial r}$ between $h \leq z \leq d$ and we shall expect that its numerical value approaches a constant value as N increases. Theoretically, this should really approach zero, but never does because of the Gibbs phenomenon that will be discussed below. Indeed, Fig. 3 shows

1. that the solution converges quickly with mode number N—no more than 30 terms are required in the series expansion to guarantee a convergent solution, and
2. that the boundary condition at $r = a$ cannot be satisfied exactly with the current approach. This is the same phenomenon as we observed for the diffraction problem in satisfying this boundary condition (cf. [15]).

Figures 4–7 show more explicitly how well the no-flux boundary condition at $r = a$ is satisfied. For the boundary condition to be satisfied exactly one would expect $\frac{\partial \psi_m}{\partial r}$ to be exactly equal to zero for $h \leq z \leq d$, however this is clearly not the case. The figures show clearly that the solution has converged after the summation of the

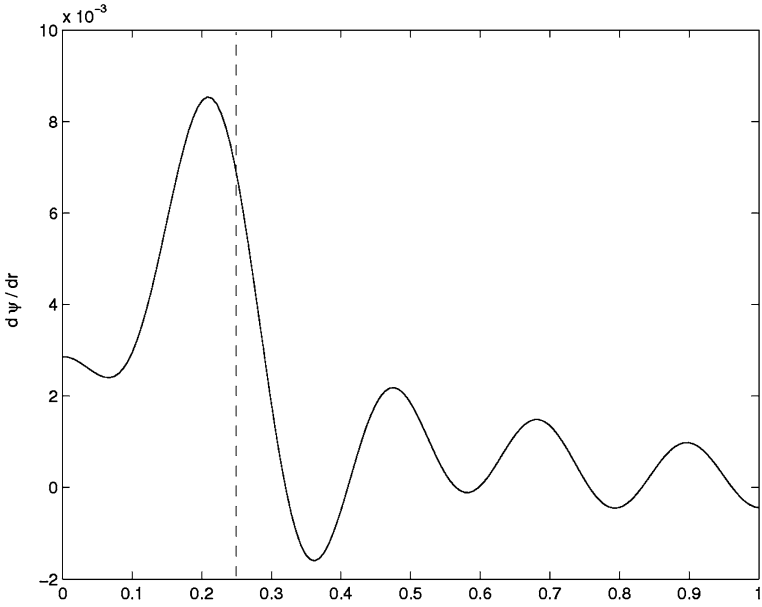

(a) $N = 10$.

Fig. 4 $\frac{\partial \psi_{\text{int}}}{\partial r}$ at $r = a$ as a function of z, for $d/a = 2$ and $h/a = 0.5$

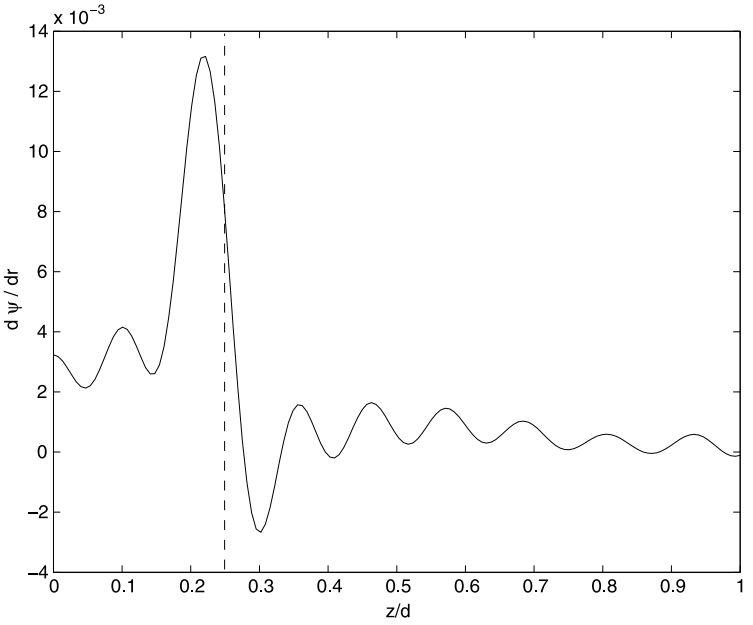

(a) $N = 20$.

Fig. 5 $\frac{\partial \psi_{\text{int}}}{\partial r}$ at $r = a$ as a function of z, for $d/a = 2$ and $h/a = 0.5$

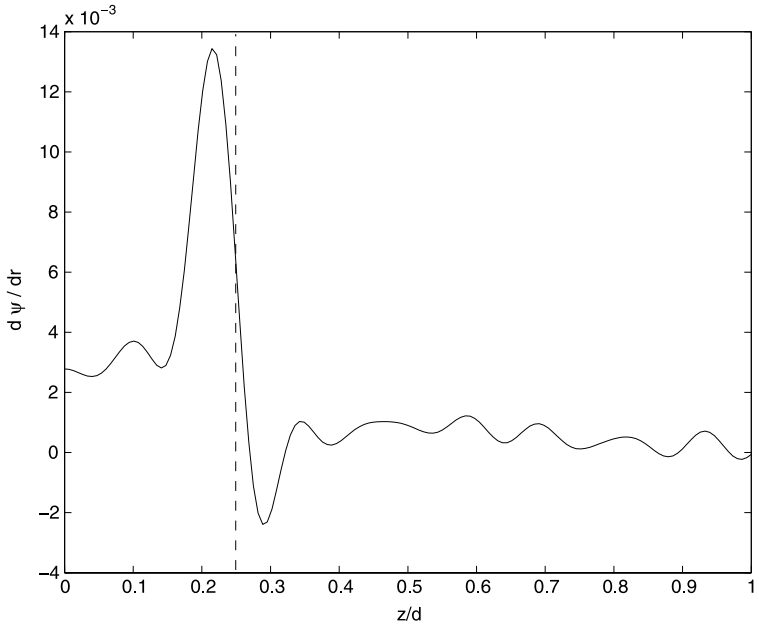

(a) $N = 40$.

Fig. 6 $\frac{\partial \psi_{\text{int}}}{\partial r}$ at $r = a$ as a function of z, for $d/a = 2$ and $h/a = 0.5$

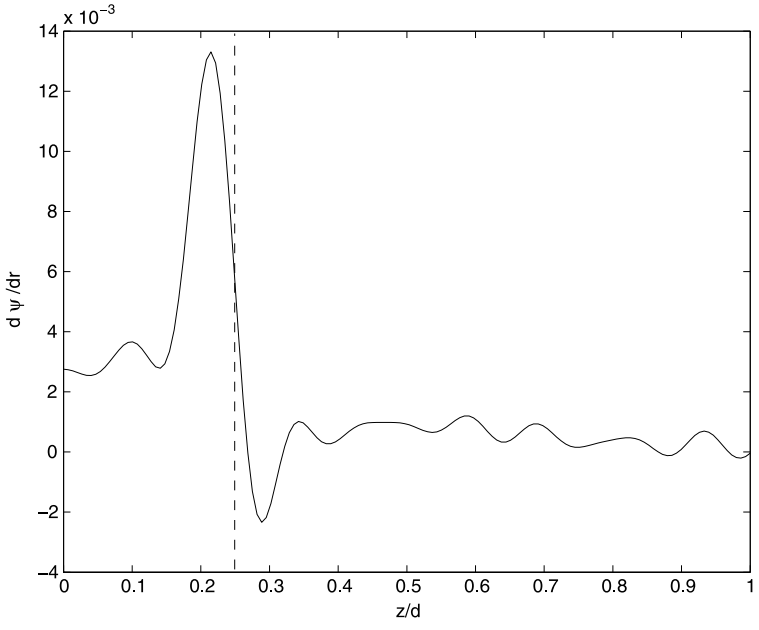

(a) $N = 60$.

Fig. 7 $\frac{\partial \psi_{\text{int}}}{\partial r}$ at $r = a$ as a function of z, for $d/a = 2$ and $h/a = 0.5$

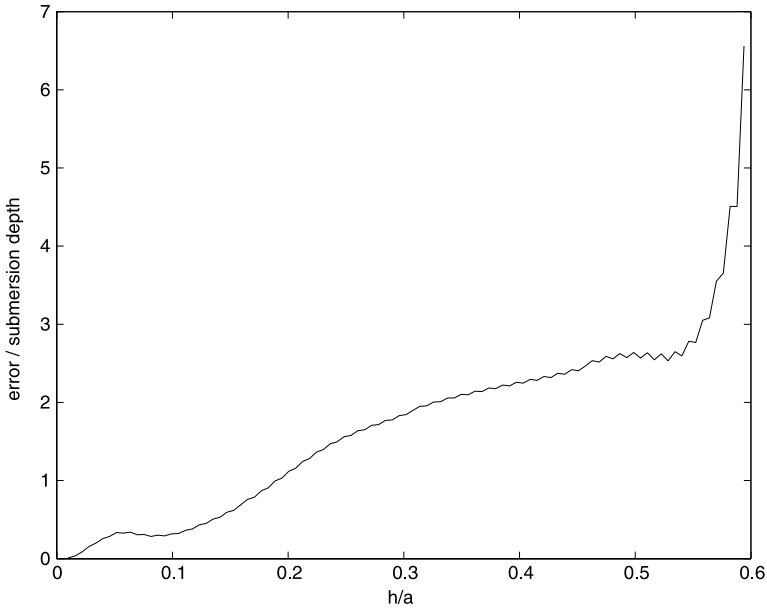

Fig. 8 Error per unit submersion depth as a function of h/a

first 40 terms, confirming the results shown in Fig. 3. However the solution does not converge to represent perfect no-flux. The peak near the lower edge of the cylinder, $z = h$, is due to Gibbs phenomenon [1], and occurs because of the discontinuity in the solution at this point.

Although this phenomenon is unavoidable as far as the current solution approach is adopted, we can measure how the large the error is and how it depends upon the cylinder submergence. Figure 8 shows a measure of the error per unit submergence depth defined by

$$\frac{\sum_{z\in[h,d]} |\frac{\partial\psi(a,z)}{\partial r}|}{d-h},$$

as a function of cylinder height off the ocean floor h. As in the diffraction problem, the figure shows that the error due to Gibbs phenomenon is worse for shallower submergences than it is for deeper submergence.

We present plots of the radiated surface wave heights ζ in metres for spatially uniform and spatially non-uniform inner surface pressure distributions. For the spatially non-uniform case we choose the surface pressure distribution

$$P(r) = P_0 \cos^2\left(\frac{2\pi r}{a}\right), \tag{39}$$

which has the average value of $\frac{P_0}{2}$ for comparison with the spatially uniform case. The results for the uniform and non-uniform cases are presented in Figs. 9 and 10 respectively. As expected, the wave heights for the non-uniform case are approximately half the height of those for the spatially uniform inner surface pressure case.

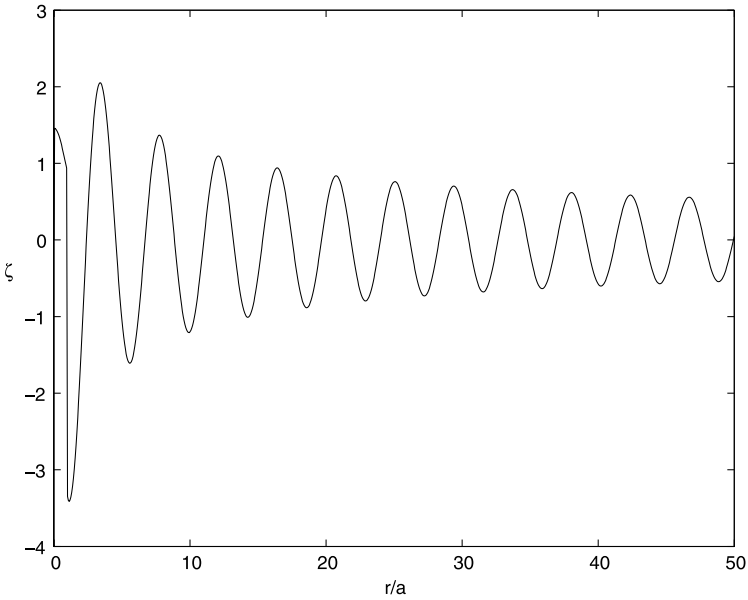

Fig. 9 Radiated wave profile along the line $\theta = 0$, spatially uniform surface pressure

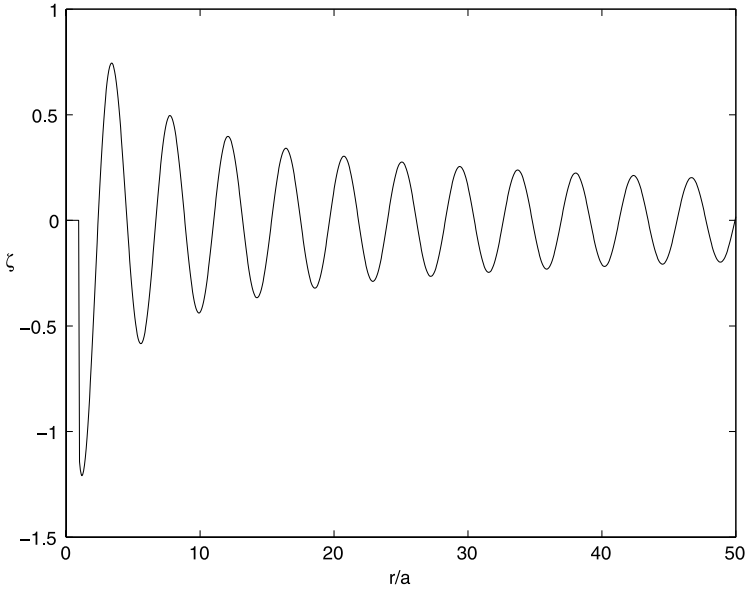

Fig. 10 Radiated wave profile along the line $\theta = 0$, $P_0(r) = P_0 \cos^2(\frac{2\pi r}{a})$

Finally, Fig. 11 shows an example of combined diffraction-radiation wave field $\zeta^{D,R}$ around the cylinder, using

$$\zeta^{D,R} = \zeta^D + \zeta^R,$$

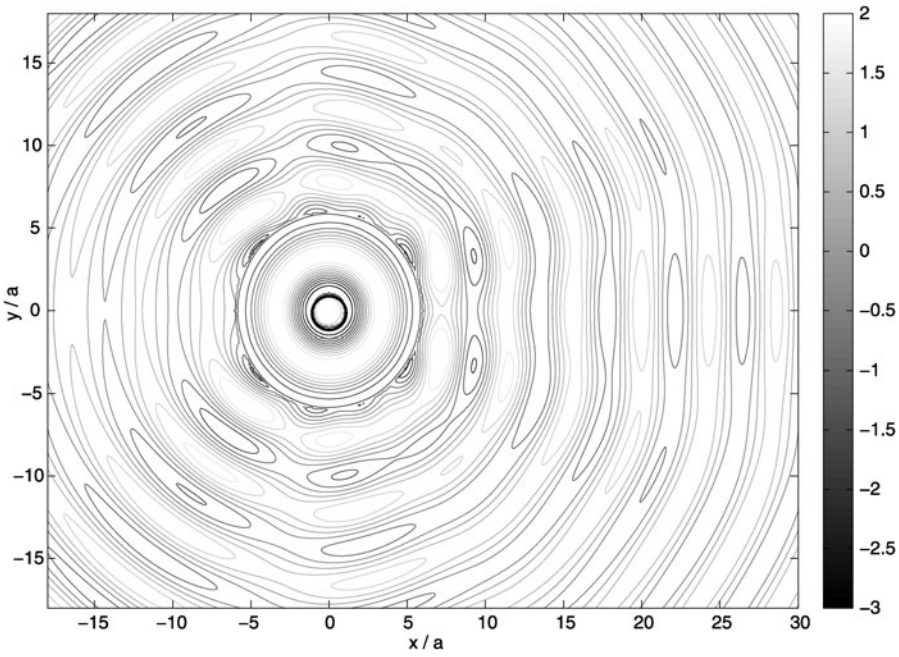

Fig. 11 Example combined diffraction-radiation wave field, using $P_0 = \text{constant}$

where ζ^D is the solution to the diffraction problem presented in the previous paper [15], and ζ^R is the solution to the radiation problem found in this paper. Here we use $P_0 = \text{constant}$, with all parameter values as given above. For comparison, the diffracted wave field is the same one plotted in Fig. 11 of [15]. In Fig. 11 presented here, only the diffracted and radiated waves are shown, while the incident plane waves traveling left to right have deliberately left out in order to show the reaction wave field alone. The figure clearly demonstrates that for the parameter values we have chosen here, the radiated waves dominate near the cylinder, however in the far-field it is the waves diffracted by the incoming wave field which are prominent. This suggests that around an OWC device radiation effects from the internal turbine are a local effect around the structure, which may still need to be considered, but are less important in the far-field around the device.

5 Conclusions

We have found an exact analytical solution for the combined problem of diffraction and radiation of surface waves around a suspended hollow cylinder in terms of an infinite series expansion. We find that our solution converges quickly, and is reasonably accurate over a range of parameter values. We find that Gibbs phenomenon has some effect on how well the no-flux boundary condition on the wall of the cylinder is satisfied for this particular solution approach, and examine how this error depends upon

on the cylinder submergence. For deeper submergences the effect of Gibbs phenomenon is minimal, and is dominant only for very shallow submergence depths, making the solution generally accurate for most depths of cylinder submersion.

We find that for the combined diffraction-radiation problem radiation effects are dominant in the near-field around the structure, while for the far-field it is the diffracted surface wave that has the larger amplitude and effect.

References

1. Arfken, G.: Mathematical Methods for Physicists. Harcourt Academic, London (2001)
2. Evans, D.V.: Wave-power absorption by systems of oscillating surface pressure distributions. J. Fluid Mech. **114**, 481–499 (1982)
3. Evans, D.V., Porter, R.: Efficient calculation of hydrodynamic properties of OWC-type devices. J. Offshore Mech. Arct. Eng. **119**(4), 210–218 (1997)
4. Falnes, J.: Ocean Waves and Oscillating Systems. Cambridge University Press, New York (2002)
5. Garrett, C.J.R.: Bottomless harbours. J. Fluid Mech. **43**(3), 433–449 (1970)
6. Hong, D.C., Hong, S.Y., Hong, S.W.: Numerical study of the motions and drift force of a floating OWC device. Ocean Eng. **31**, 139–164 (2004)
7. Lighthill, J.: Two-dimensional analyses related to wave-energy extraction by submerged resonant ducts. J. Fluid Mech. **91**, 253–317 (1979)
8. Martins-Rivas, H., Mei, C.C.: Wave power extraction from an oscillating water column at the tip of a breakwater. J. Fluid Mech. **626**, 395–414 (2009)
9. Mei, C.C.: The Applied Dynamics of Ocean Surface Waves. World Scientific, Singapore (1994)
10. Miles, J.W.: On surface-wave radiation from a submerged cylindrical duct. J. Fluid Mech. **122**, 339–346 (1982)
11. Sarmento, A.J.N.A., de O. Falcao, A.F.: Wave generation by an oscillating surface-pressure and its application in wave-energy extraction. J. Fluid Mech. **150**, 467–485 (1985)
12. Simon, M.J.: Wave-energy extraction by a submerged cylindrical duct. J. Fluid Mech. **104**, 159–187 (1981)
13. Stoker, J.J.: Water Waves: The Mathematical Theory with Application. Wiley-Interscience, New York (1957)
14. Wehausen, J.V., Laitone, E.V.: Surface waves. In: Encyclopaedia of Physics, vol. IX, pp. 446–778. Springer, Berlin (1960)
15. Zhu, S.-P., Mitchell, L.: Linear diffraction of ocean waves around a hollow cylindrical shell structure. Wave Motion **46**, 78–88 (2009)